Electronic Supplementary Material (ESI) for Physical Chemistry Chemical Physics.

Supporting Information

Revealing the Role of Phosphoric Acid in All-Vanadium Flow Batteries with DFT Calculations and *In situ* Analysis

Fabio J. Oldenburg, Marta Bon, Daniele Perego, Daniela Polino, Teodoro Laino, Thomas J. Schmidt and Lorenz Gubler

Abstract The present work suggests the use of a mixed water-based electrolyte containing sulfuric and phosphoric acid for both negative and positive electrolytes of a vanadium redox flow battery. Computational and experimental investigations reveal insights on the possible interactions between the vanadium ions in all oxidation states and sulphate, bisulphate, dihydrogen phosphate ions and phosphoric acid. *In situ* cycling experiments and ion-specific electrochemical impedance measurements confirmed a significant lowering of the charge-transfer resistance of the reduction of V(III) ions and consequent increase of the voltaic efficiency associated with the negative side of the battery. This increase of performance is attributable to the complexation of this oxidation state by phosphoric acid. So far, mixed acids have mainly been discussed with the focus on V(V) solubility. In this work we rationalize the impact of the mixed acids on the electrochemical efficiency opening new strategies on how to improve the cycling performance with ionic additives.

Validation of Electrochemical Impedance Spectroscopy

For validation, the sum of the polarization resistance obtained from both half-cells separately was compared to the resistance obtained for the full cell set-up. Both resistances were obtained from the x-axis intersection of the fitted curve. The fit was calculated based on an ohmic resistance (R_S) and an electrochemical double-layer, the latter represented with a polarization resistance (R_{CT}) in parallel with a constant phase element (CP) (Figure S1).

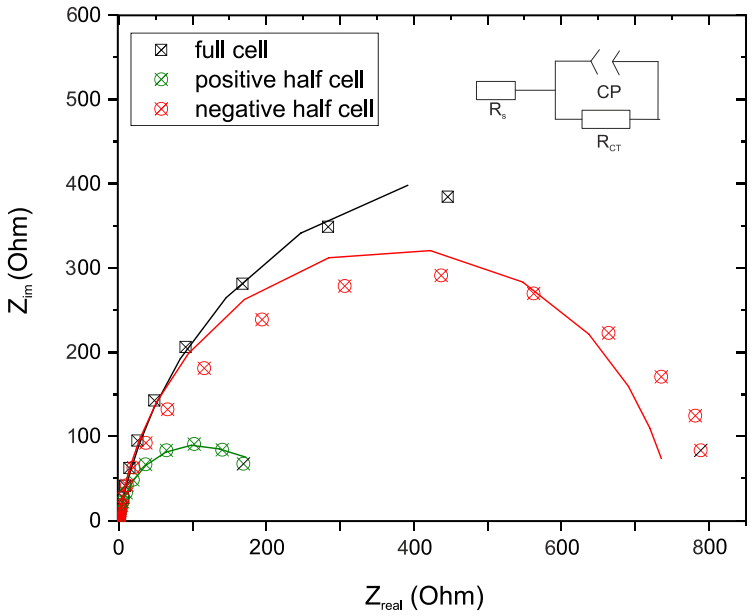

Figure S1. Electrochemical impedance spectra of a fully discharged vanadium flow battery cell (determined between 100 kHz-1 mHz at 0 V vs. open circuit potential with a voltage amplitude of 100 mV). The full cell impedance was measured between the two half-cells, whereas the impedance of one half-cell was measured with a Hg/Hg_2SO_4-reference electrode (edge-type set-up, 2 M H_2SO_4 electrolyte).

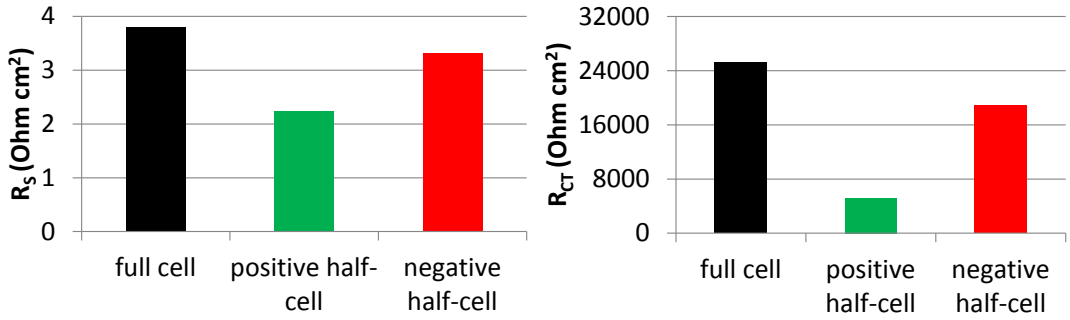

Figure S2. Polarization and ohmic resistance of the full cell and each half-cell, respectively, determined from the x-axis intersection of the fitted nyquist plot from figure S1.

Configurations

The compressed file configurations.tar.gz contains the structures reported in Schemes 1- 4 of the manuscript, in .xyz format, named after Scheme S1.

Experimental Raman Spectra

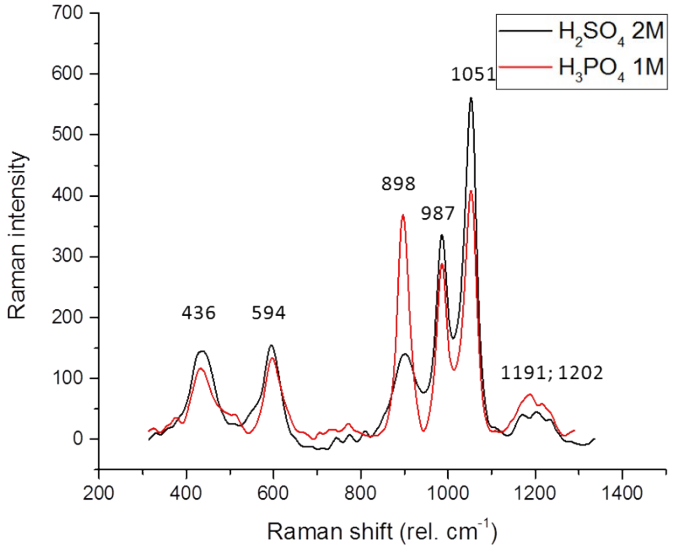

H_3PO_4	1170; 891
$H_2PO_4^-$	1078
HPO_4^{2-}	990
HSO_4^-	1051; 898
SO_4^-	1200; 987, 594, 436

Figure S3. Raman spectra of a solution of 2 M sulphuric acid (black) and 1 M phosphoric acid (black) with the assigned Raman shifts.[1]

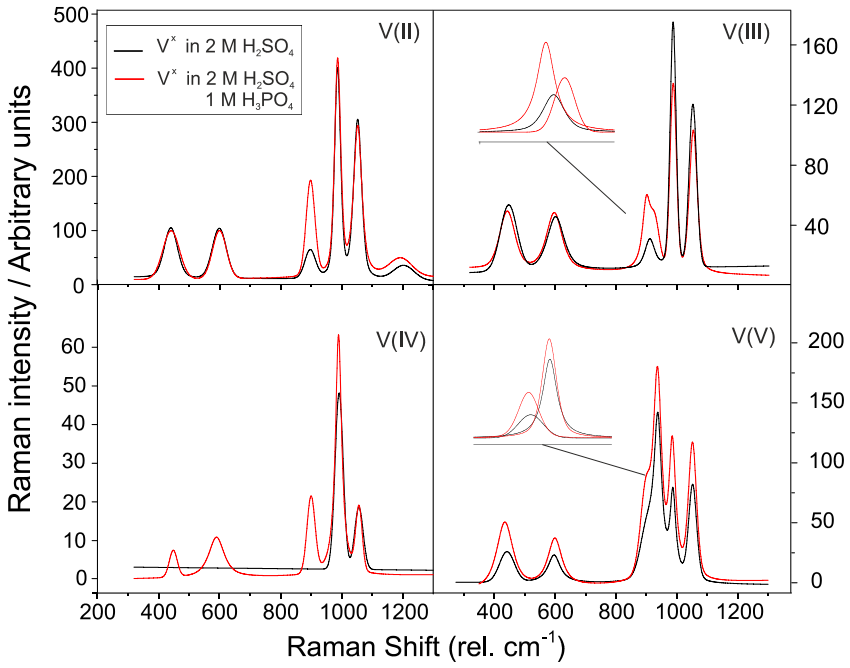

Figure S4. Raman spectra of vanadium II-V dissolved in 2 M sulphuric acid (black) and in a mixed acid solution of 2 M sulphuric acid and 1 M phosphoric acid.

Computational Raman Spectra

The Raman spectra calculated for the configurations of V^{2+} with the lowest energy in the vicinity of sulfate and phosphate groups are shown in Figures S5 and S9. The ones for V^{3+} are shown in Figures S6 and S10, while Raman spectra for VO^{2+} are reported in Figures S7 and S11. Finally, Raman spectra for configurations of VO_2^+ are shown in Figures S8 and S12.
We comment separately two different wavenumber ranges: While the former (in Figures S5-S9), at 400-2000 cm^{-1}, is generated by O-S, O-P, O-V stretching and to the H-O-H bending, the latter (in Figures S10-S12), at 2000-4000 cm^{-1} includes mainly the O-H stretching modes.

400-2000 cm^{-1}

V^{2+}. As it can be seen from Figure S3, the H_3PO_4 / $H_2PO_4^-$ produces two distinct P-O stretching signals, the former at 799-814 cm^{-1} (symmetrical), the latter at 1146-1157 cm^{-1} (antisymmetrical). The S-O stretching signal of SO_4^{2-} (Figures S5.a and S5.c) generates two different fingerprints: at about 865 cm^{-1} (symmetrical), and 1125 cm^{-1} (antisymmetrical). In some configurations the former signal is overlapping with the corresponding H-O-S bending vibration, with the hydrogen being donated by H_2O (at 926 cm^{-1} and 865-871 cm^{-1} for Conf.1 and Conf.3, respectively). This H-O-S bending vibration is not visible in Figure S5.c, but is present in Figure S5.d, referring to the H-bond between HSO_4^- and H_2O (shifted to 719-770 cm^{-1}). Within the protonation of SO_4^{2-}, the symmetrical O-S stretching is shifted to higher wavenumbers (from 865 cm^{-1} to 966-971 cm^{-1}). However, the absorption of the antisymmetrical stretching vibration remains largely unaffected.
When comparing the signals from the free additives compared to the ones which are present in the first solvation shell of vanadium we noticed the following:

1. No shift is visible from the case in which the additive is free (Confs. 1 and 2) compared to the case in which it is complexing V^{2+} (Confs. 3 and 4).
2. No new signal appears when the additives are bound to vanadium.

V^{3+}. In Figure S4 the P-O stretching fingerprints of H_3PO_4 / $H_2PO_4^-$ are visible, although in an energy range slightly different compared to the case of V^{2+}. In fact, the P-O stretching of H_3PO_4 can be assigned to an absorption peak in the range of 779-829 cm^{-1} (symmetrical) and 1048-1179 cm^{-1} (antisymmetrical) (Figures S6.a and S6.b). In presence of $H_2PO_4^-$ (Figures S6.c and S6.d), we observe three fingerprints: the symmetrical stretching vibration at 779-815 cm^{-1}, and two antisymmetrical stretching vibrations at 1098-1192 cm^{-1} (as for H_3PO_4) and one at 920-940 cm^{-1}.
The S-O stretching peaks SO_4^{2-} are shifted towards higher wavenumbers on the right compared to those in Figure S5. The symmetrical vibration appears within a range of 870-970 cm^{-1} whereas the antisymmetrical is within in a range of 1060-1170 cm^{-1}. Sometimes, for some configurations, the former signal is overlapping with the H-O-S bending absorption corresponding to an H-bond between one H_2O and a SO_4^{2-}-ion (900-930 cm^{-1}). Moreover, we noticed that a third peak appears when $SO4^{2-}$ is bound to V^{3+} at about 600 cm^{-1}. As for the V^{2+} case, the symmetrical O-S stretching is shifted towards higher wavenumbers after the protonation of SO_4^{2-} and the formation of HSO_4^-(from 870 cm^{-1} to about 960 cm^{-1}). In contrast to V^{2+}, in Figure S6 we observe a third peak corresponding to the S-OH bond stretching of HSO_4^- at lower wavenumbers (680-793 cm^{-1}). Furthermore, an intense absorption peak appears at 587 cm^{-1}, which corresponds to the V-OH stretching vibration.
When analyzing how the signals shift between the free additives and the bound ones we made the following observations.
Case A:

- No shift is observed from the absorption peak of free additive (Confs. 1 and 2) to the absorption peaks of complexing additives (Confs. 3 and 4)

Case B:

- the absorption assigned to the free symmetrical H_3PO_4 bond stretching at about 800 cm^{-1} is slightly blue-shifted to 830 cm^{-1} in the bound state (Confs. 3 and 4).
- The absorption assigned to the free antisymmetrical H_3PO_4 bond stretching vibration at about 1180 cm^{-1} is red-shifted (1048-1105 cm^{-1}) in the bound state (Confs. 3 and 4).
- The absorption assigned to the S-OH bond stretching vibration of HSO_4^- in the free state (Confs. 1 and 3), at about 680-690 cm^{-1}, shifts to the right at 780-750 cm^{-1} for Conf.2 and Conf.4.
- The signal assigned to the free symmetrical HSO_4^- S-O bond stretching is located at 964 cm^{-1} (Confs. 1 and 3) and red-shifts to 906-916 cm^{-1} when complexing V^{3+} (Confs. 2 and 4).
- The signal corresponding to the antisymmetrical HSO_4^- vibration at 1060-1044 cm^{-1} gets more intense when complexing V^{3+} (Confs. 2 and 4).

Case C

- No shift is visible for the $H_2PO_4^-$ additive.

- The signal corresponding to the free symmetrical stretching of SO_4^{2-} is found at 877 cm^{-1} (Conf.1). This signal however shifts towards higher wavenumbers (946 cm^{-1}), when it is complexing V^{3+} (Conf.2).
- The signal corresponding to the antisymmetrical SO_4^{2-} vibration does not shift significantly, but is intensified when the additive is bound to V^{3+} (Confs.2 and 4).

Case D

- No shift is visible for the $H_2PO_4^-$ additive.
- The signal corresponding to the HSO_4^- antisymmetrical mode at 1054 cm^{-1} is more evident when complexing V^{3+} (Conf.4)

VO^{2+}. Many similarities are found between the calculated spectra of V^{3+} (Figure S6) and of VO^{2+} (Figure S7). In this case, again two distinct signals corresponding to the P-O stretching vibrations of H_3PO_4 are visible. The symmetrical one is located between 777-835 cm^{-1}, while the antisymmetrical appears between 1078-1182 cm^{-1}. For $H_2PO_4^-$ we observe three signals: One corresponding to the symmetrical stretching at 798-812 cm^{-1} and two referring to the antisymmetrical stretching, at 1090-1171 cm^{-1} (similarly to H_3PO_4) and at 937-1001 cm^{-1}. The S-O stretching of SO_4^{2-} (Figures S7.a and S7.c) generates two different fingerprints in the wavenumber ranges of 830-947 cm^{-1} (symmetrical) and 1130-1160 cm^{-1} (antisymmetrical). The former signal overlaps with the one corresponding to the H-O-S bending vibration at 1072-1098 cm^{-1} (Conf.3 in Figure S7.c) and at 970-1018 cm^{-1} (Conf.3 in Figure S7.a). The same signal is present also in Figure S7.b, although produced by the H-bonding between HSO_4^- and H_2O and shifted towards lower wavenumbers (745-799 cm^{-1}). Noticeably, as for Figure S6, also in this case a third signal is visible when SO_4^{2-} complexes VO^{2+}. This signal however, is blue-shifted compared to Figure S6, moving from 600 cm^{-1} to 755-848 cm^{-1}. As we have observed in Figures S5 and Figure S6, the symmetrical S-O stretching vibration of HSO_4^- shifts to higher energies compared to SO_4^{2-}, (from 830-947 cm^{-1} to 892-973 cm^{-1}), while the signal of the antisymmetrical stretching vibration appears at 1042-1075 cm^{-1} only when HSO_4^- complexes VO^{2+} in Confs.2 and 4 of Figure S7.d. Similarly to the case of Figure S6, again we observe a third peak corresponding to the S-OH bond stretching of HSO_4^- at lower wavenumbers (699-757 cm^{-1}).

Furthermore, in the case of VO^{2+} an additional fingerprint appears in the range of 985-1084 cm^{-1} corresponding to the stretching vibration of the V-O bond.

The following differences are observed between the spectra containing the free additives and the ones with bound additives:

Case A:

- The signal assigned to the free symmetrical H_3PO_4 bond stretching at about 780 cm^{-1} is blue-shifted to 830 cm^{-1} in the bound state (Confs. 3 and 4).
- The signal assigned to the free antisymmetrical H_3PO_4 bond stretching at about 1170-1180 cm^{-1} is shifted to lower wavenumbers (1074-1078 cm^{-1}) in the bound state (Confs. 3 and 4).
- The signal corresponding to the free symmetrical stretching of SO_4^{2-} is found between 830-870 cm^{-1} (Confs. 1 and 3). This signal however shifts towards higher wavenumbers (900-946 cm^{-1}), when it is complexing VO^{2+} (Confs. 2 and 4).
- The signal corresponding to the antisymmetrical SO_4^{2-} vibration does not shift significantly.
- A new signal appears when SO_4^{2-} is bound to VO^{2+} at 755 cm^{-1} for Conf.2 and at 848 cm^{-1} for Conf.4.
- The V-O stretching signal shifts in Conf.4, from 1035-1053 cm^{-1} to 970-1010 cm^{-1}, overlapping with the signal produced by the H-bonding between SO_4^{2-} and H_2O.

Case B:

- The signal assigned to the free symmetrical H_3PO_4 bond stretching at about 804-818 cm^{-1} is shifted to a slightly higher wavenumber range (830-835 cm^{-1}) in the bound state (Confs. 3 and 4).
- The signal assigned to the free antisymmetrical H_3PO_4 bond stretching between 1150-1160 cm^{-1} is red-shifted (1080-1090 cm^{-1}) in the bound state (Confs. 3 and 4).
- The signals assigned to the S-OH bond stretching of HSO_4^- do not show any significant shift.
- The signal assigned to the free symmetrical HSO_4^- S-O bond stretching is located at 964 cm^{-1} (Confs. 1 and 3) and shifts to a lower wavenumber of 923 cm^{-1} when it complexes the VO^{2+}-ion alone (Conf. 2). The same shift is not observed when both H_3PO_4 and HSO_4^- are bound to VO^{2+}.
- The V-O stretching signal is found at higher energies compared to Case A (1084 cm^{-1}) in the unbounded state. Moreover, when H_3PO_4 complexes VO^{2+} the VO signal shifts to a lower wavenumber of 1048 cm^{-1} which is found to be even lower when both H_3PO_4 and HSO_4^- are present in the first solvation shell (1018 cm^{-1}).

Case C

- The antisymmetrical signal of $H_2PO_4^-$ in the unbound state is located at 951 cm^{-1}. Interestingly, this signal does not shift in comparison to the unbound state of $H_2PO_4^-$, however it is shifted to higher energies when SO_4^{2-} is bounded to VO^{2+}(994 cm^{-1} for Conf.2 and to 1023 cm^{-1} for Conf.4).
- The signal corresponding to the free symmetrical stretching of SO_4^{2-} is found at 885 cm^{-1} (Conf.1). This signal however shifts towards higher wavenumbers (929 cm^{-1}) when it is complexing VO^{2+} (Confs.2 and 4).

- A new signal appears when SO_4^{2-} is bound to VO^{2+} at 791 cm^{-1} for Conf.2 and at 806 cm^{-1} for Conf.4.
- The signal corresponding to the V-O stretching is located between 1051-1058 cm^{-1} in all configurations except for Conf.4, for which this signal is shifted towards lower wavenumbers (985 cm^{-1}) and overlaps with the antisymmetrical P-O-stretching vibration of $H_2PO_4^-$.

Case D

- One of the antisymmetrical signal of $H_2PO_4^-$ in the unbound state is located at 974 cm^{-1}. Interestingly, this signal appears not to be shifted in comparison to the bound state of $H_2PO_4^-$, except for the case when HSO_4^- is bounded to VO^{2+} (here moving to higher energies if only HSO_4^- is bound (1001 cm^{-1} for Conf.2) and to lower energies when both additives complex VO^{2+} (937 cm^{-1} for Conf.4).
- The signal assigned to the free symmetrical S-O-bond-stretching of HSO_4^- is located at a range of 958-973 cm^{-1} (Confs.1 and 3) and is shifted towards lower wavenumbers of 892-914 cm^{-1} when it complexes VO^{2+} (Confs.2 and 4).
- The signals assigned to the S-OH bond stretching of HSO_4^- in the free state (Confs.1 and 3), between 699-706 cm^{-1}, shift to 831 cm^{-1} for Conf.2 and 757 cm^{-1} for Conf.4 of Figure S3.d.
- The location of the V-O signal does not vary from the unbound to the bound state. However, when HSO_4^- (Conf.2) or $H_2PO_4^-$ (Conf.3) are bound the signal width increases as it overlaps with the internal S-O and P-O stretching modes of the two additives.

VO_2^+. As found for the previous cases, we observe two signals corresponding to H_3PO_4: the symmetrical P-O stretching vibration located in the wavenumber range of 807-853 cm^{-1} and the antisymmetrical vibration located in the range of 989-1148 cm^{-1}. A third peak appears when H_3PO_4 complexes VO_2^+ in Confs.3 and 4 of Figure S8.b at 999 and 909 cm^{-1} respectively. For $H_2PO_4^-$ again we observe three peaks: the former corresponds to the symmetrical stretching of the P-O bond, and is similar to that of H_3PO_4, at 796-848 cm^{-1}. The other two signals correspond to the antisymmetrcal stretching vibrations and are located between 1096-1203 cm^{-1} (similarly to H_3PO_4) and between 910-1009 cm^{-1}. It is interesting to note that in Conf.4 of Figure S8.a we observe another peak associated to $H_2PO_4^-$ at 692 cm^{-1}. This signal corresponds to the P-OH-V vibration, and it can be associated to this peculiar case in which the phosphorus atom bonds vanadium through an OH group and not a simple oxygen atom. Similar to H_3PO_4, also for the coordination of $H_2PO_4^-$ (Confs.3 and 4) a new stronger peak appears in the range of 879-922 cm^{-1} which corresponds to the P-OV stretching.
Three peaks for the S-O stretching vibration produced by SO_4^{2-} are visible. One associated with the symmetrical stretching at a range of 935-960 cm^{-1} and two referring to the antisymmetrical stretching vibration (1071-1110 $cm^{-1}$and 1155-1168 cm^{-1}). Moreover, we noticed that another peak appears when SO_4^{2-} is bounded to VO_2^+ at about 620-768 cm^{-1}. Considering HSO_4^-, the symmetrical S-O stretching is observed between 922-959 cm^{-1}. Often this signal overlaps with the one corresponding to the bending of the hydrogen bond between HSO_4^- and H_2O (940-968 cm^{-1}). Two antisymmetrical S-O stretching vibrations are found also in this case, which are located at 1052-1113 cm^{-1} and 1165-1240 cm^{-1}. Similar to what we observed in previous cases, also here another peak appears at 714-809 cm^{-1} that corresponds to the stretching vibration of the S-OH bond.
In the case of VO_2^+, two additional signals are visible: one at 890-982 cm^{-1} corresponding to the antisymmetrical V-O stretching and one at 989-1051 cm^{-1} corresponding to the symmetrical stretching vibration of the V-O bond.
In the comparative analysis of the bound and the unbound states, it is important to underline that the sulfate group in the unbound state is always protonated after the geometry optimization calculation. For this reason we do not have information about the signals of the free SO_4^{2-} and we cannot discern if a shift between the free and the bound state occurs. In this framework, we made the following observations.
Case A:

- Passing form the free to the bound state, H_3PO_4 loses one H atom becoming $H_2PO_4^-$ and hence a direct comparison is not possible. However, since the signal assigned to the symmetrical free $H_2PO_4^-$ is very close to that of H_3PO_4, we may still notice a shift. In fact, in the bound state (Confs. 3 and 4) the symmetrical P-O stretching of $H_2PO_4^-$ is blue-shifted and appears in the range of 824-848 cm^{-1}.
- Additionally in this case a direct comparison between the free and the bound antisymmetrical H_3PO_4 bond stretching is not possible. The signal assigned to the free antisymmetrical H_3PO_4 is located at about 1140 cm-^{1}. However in the bound state, passing from H_3PO_4 to $H_2PO_4^-$ we find one lower wavenumber at 1118 cm^{-1}, when only $H_2PO_4^-$ complexes VO_2^+ and a higher one at 1203 cm^{-1}, when both $H_2PO_4^-$ and SO_4^{2-} are complexing the vanadium oxide.
- A new signal appears when SO_4^{2-} is bound to VO^{2+} at 768 cm^{-1} for Conf.2 and at 747 cm^{-1} for Conf.4.
- No shifts are observed for the V-O signals.

Case B:

- The signal assigned to the free symmetrical H_3PO_4 bond stretching at about 807-814 cm^{-1} is blue-shifted (853-839 cm^{-1}) in the bound state (Confs. 3 and 4).
- The signal assigned to the free antisymmetrical H_3PO_4 bond stretching in the range of 1135-1148 cm^{-1} is red-shifted (989 and 1082 cm^{-1} in Confs. 3 and 4, respectively).

- A new signal appears when H_3PO_4 complexes the vanadium oxide at 999 and 909 cm^{-1} in Confs. 3 and 4 respectively.
- The signals assigned to the S-OH bond stretching vibration of HSO_4^- shifts from 714 and 765 cm^{-1} in the free state (Confs. 1 and 3) to 794 and 809 cm^{-1} in the VO_2^+-complexing state (Confs. 2 and 4).
- The signal assigned to the free symmetrical S-O bond stretching of HSO_4^- is located at 964 cm^{-1} (Conf. 1) and shifts to lower wavenumbers (839-854 cm^{-1}) when it complexes VO^{2+} (Confs. 2 and 4).
- The V-O stretching signals do not show any significant shift.

Case C:

- The signal assigned to the free symmetrical $H_2PO_4^-$ bond stretching at about 796-806 cm^{-1} is slightly blue-shifted in the bound state (823-835 cm^{-1}, Confs. 3 and 4).
- The antisymmetrical signal of $H_2PO_4^-$ in the unbound state located at 1004 cm^{-1} is red-shifted when $H_2PO_4^-$ only, SO_4^{2-} or both are bounded to VO_2^+ (890-915 cm^{-1}).
- New signals appear when $H_2PO_4^-$ complexes the vanadium oxide at 877 and 892 cm^{-1} in Conf.3 and Conf.4 respectively.
- A new signal appears when SO_4^{2-} is bound to VO^{2+} at 748 cm^{-1} for Conf.2 and at 736 cm^{-1} for Conf.4.
- The signals corresponding to the V-O symmetrical and antisymmetrical stretching vibrations do not show any significant shift.

Case D:

- The signal assigned to the free symmetrical $H_2PO_4^-$ bond stretching at about 814-820 cm^{-1} is slightly blue-shifted in the bound state (831-848 cm^{-1} Confs. 3 and 4).
- The antisymmetrical signal of $H_2PO_4^-$ in the unbound state located at 976-982 cm^{-1} shifts when $H_2PO_4^-$ is bound to VO_2^+ and is found at 910 cm^{-1}.
- A new signal appears when $H_2PO_4^-$ complexes the vanadium oxide at 892 and 879 cm^{-1} in Confs. 3 and 4 respectively.
- A new signal appears when SO_4^{2-} is bound to VO^{2+} at 620 cm^{-1} for Conf.2 and at 723 cm^{-1} for Conf.4.
- The signals corresponding to the V-O symmetrical and antisymmetrical stretching vibration do not show any significant shift.

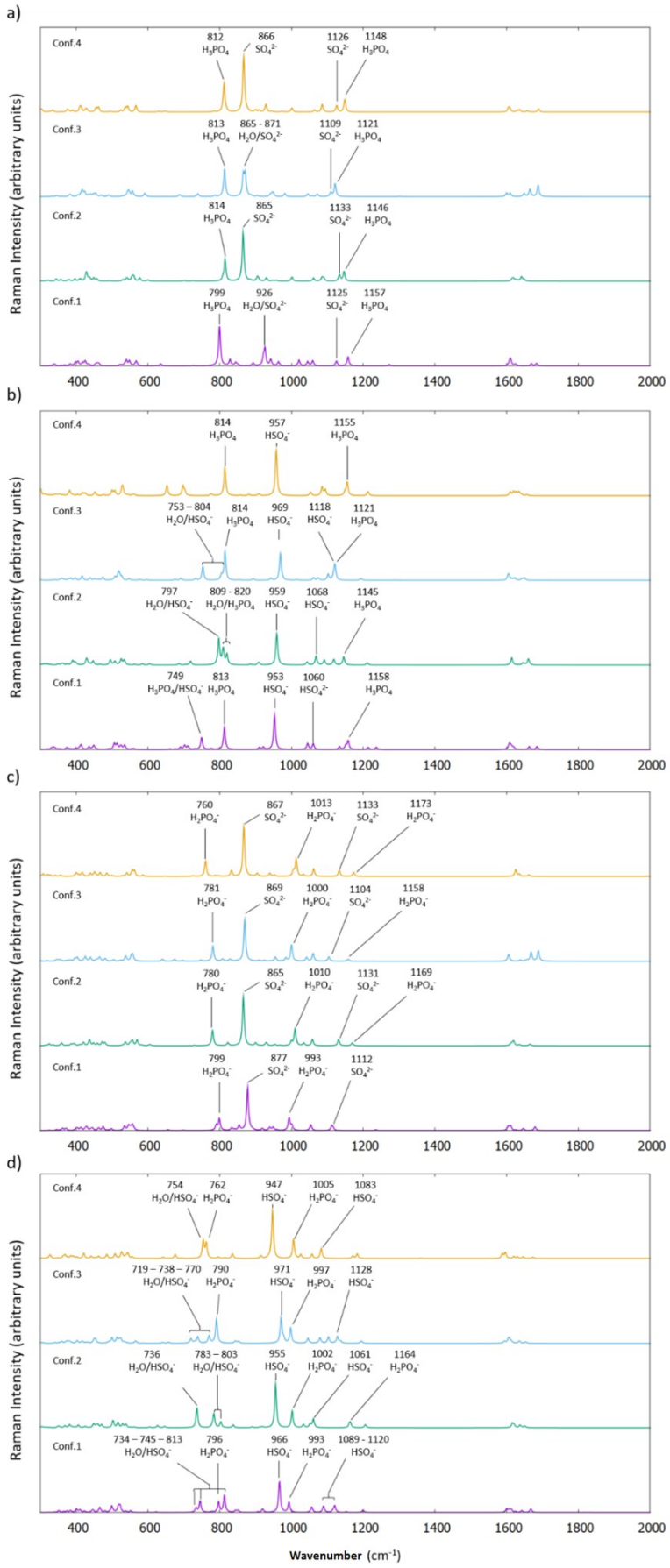

Figure S5 a) Computational Raman Spectra in the 400-2000 cm^{-1} range for the V^{2+} cation within the vicinity of SO_4^{2-} and H_3PO_4. **b)** The protonation of SO_4^{2-} is considered. **c)** The deprotonation of H_3PO_4 is shown. **d)** The protonation of SO_4^{2-} and the first deprotonation of H_3PO_4 are here represented. The most significant structures are selected on the basis of Scheme S1.

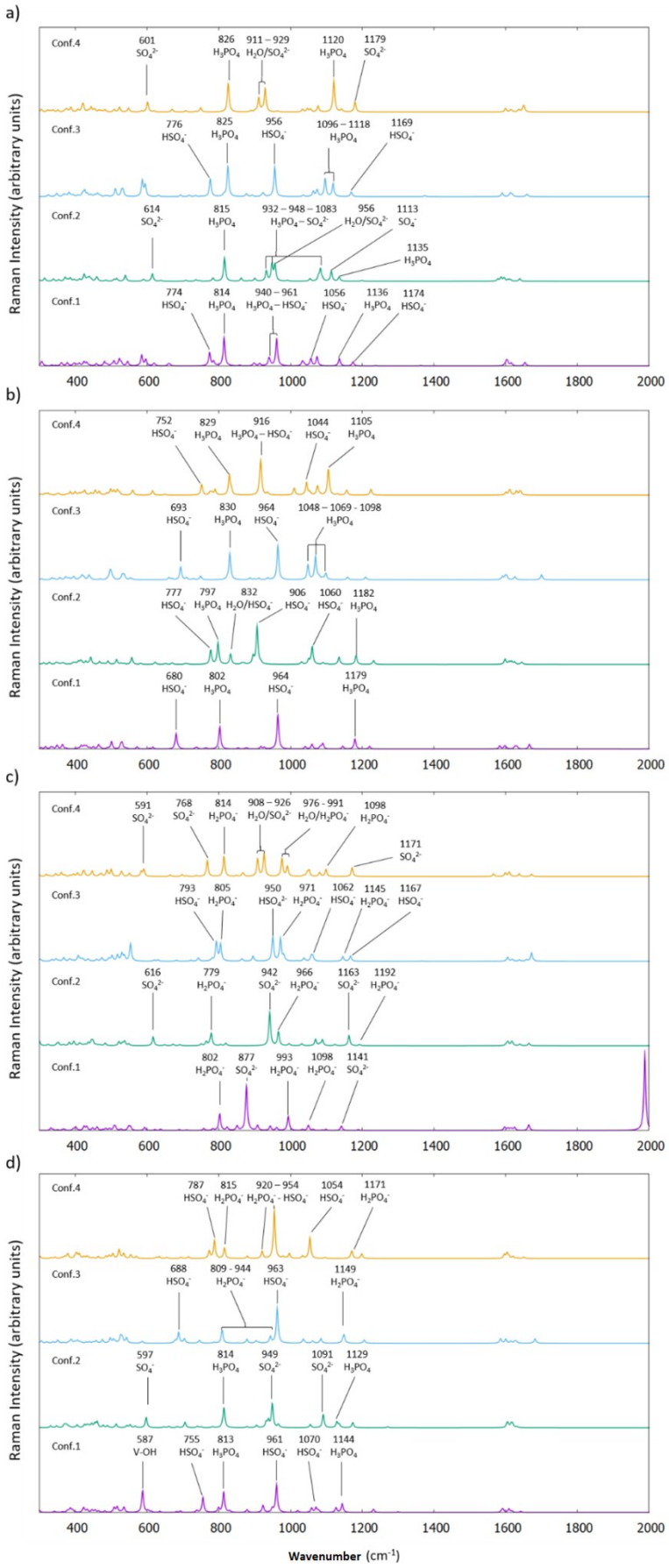

Figure S4. **a)** Computational Raman Spectra in the 400-2000 cm^{-1} range for the V^{3+} cation within the vicinity of SO_4^{2-} and H_3PO_4. **b)** The protonation of SO_4^{2-} is considered. **c)** The deprotonation of H_3PO_4 is shown. **d)** The protonation of SO_4^{2-} and the first deprotonation of H_3PO_4 are here represented. The most significant structures are selected on the basis of Scheme S1.

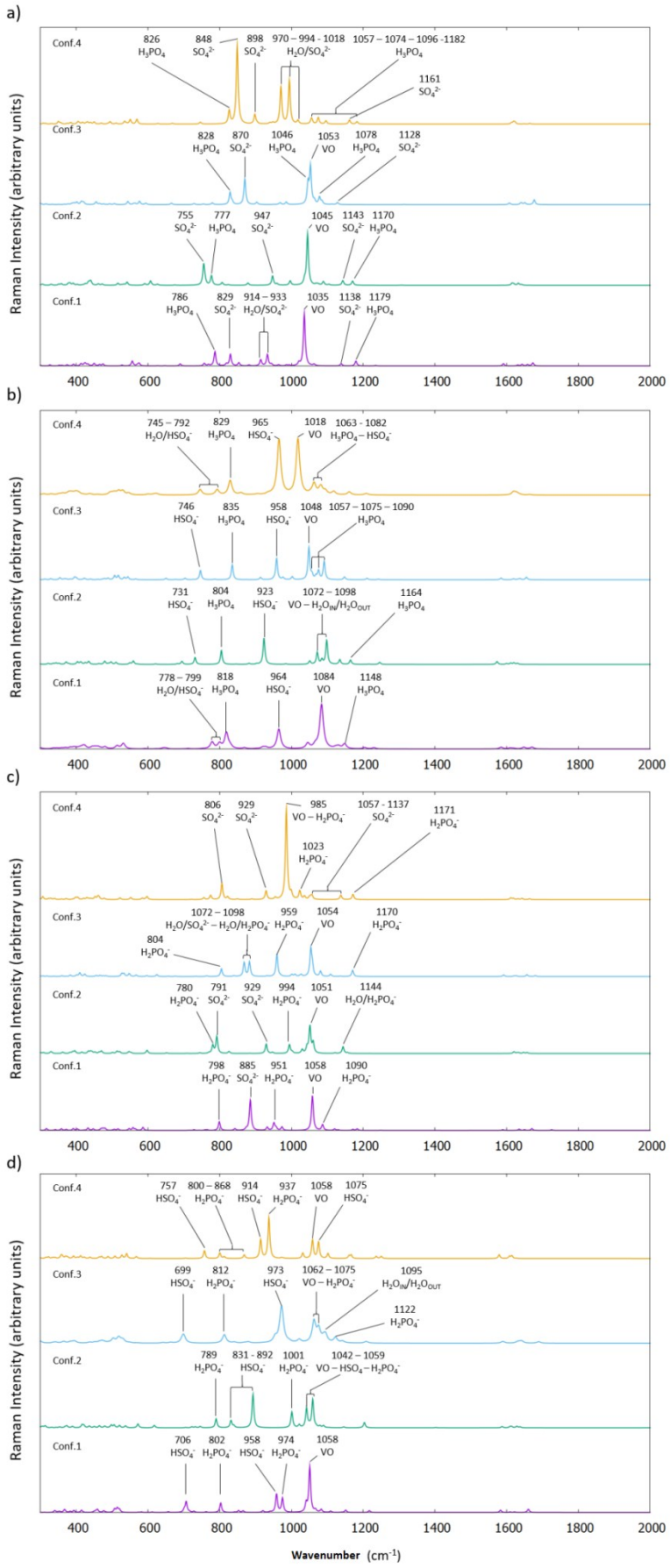

Figure S6. **a)** Computational Raman Spectra in the 400-2000 cm^{-1} range for the VO^{2+} cation within the vicinity of SO_4^{2-} and H_3PO_4. **b)** The protonation of SO_4^{2-} is considered. **c)** The deprotonation of H_3PO_4 is shown. **d)** The protonation of SO_4^{2-} and the first deprotonation of H_3PO_4 are here represented. The most significant structures are selected on the basis of Scheme S1.

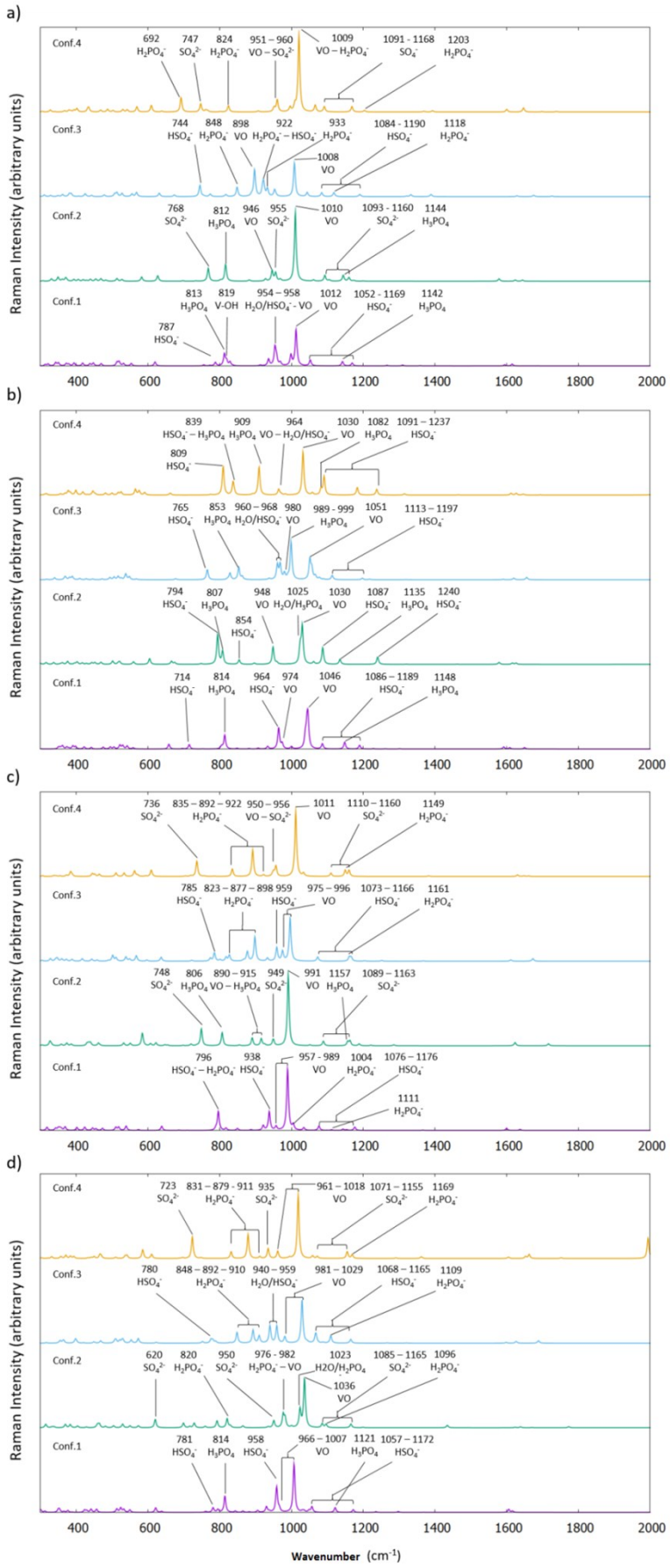

Figure S7. **a)** Computational Raman Spectra in the 400-2000 cm^{-1} range for the VO_2^+ cation within the vicinity of SO_4^{2-} and H_3PO_4. **b)** The protonation of SO_4^{2-} is considered. **c)** The deprotonation of H_3PO_4 is shown. **d)** The protonation of SO_4^{2-} and the first deprotonation of H_3PO_4 are here represented. The most significant structures are selected on the basis of Scheme S1.

2000-4000 cm^{-1}

V^{2+}. All possible configurations for V^{2+} include H-bonds between the H_2O molecules of the first solvation shell and the oxygens of the sulfate/bisulfate group in the second solvation shell (see Scheme 1 of the manuscript). As shown in Figure S9, the O-H stretching vibration of the sulfate group refers to a signal between 3000-3200 cm^{-1} in the Raman spectra. However, we noticed that when H_3PO_4 is present in the first coordination shell the signal appears to be shifted to 2900-3100 cm^{-1}. Passing from the sulfate to the bisulfate group, this signal shifts to higher wavenumbers producing a signal at 3300-3500 cm^{-1}. In the same wavenumber range also another signal appears from the H-bonds formed between the H_2O molecules outside the first solvation shell and the sulfate or bisulfate group.
The H-bonding between H_2O molecules of the first shell and the oxygens of H_3PO_4 absorbs as well in the range of 3400-3500 cm^{-1}. However, when the phosphoric acid is deprotonated to $H_2PO_4^-$ this signal shifts towards lower wavenumbers (3000-3300 cm^{-1}). Moreover, if the H-bonding occurs between a hydrogen bound to a phosphate group and an oxygen of H_2O from the first solvation shell of, the O-H stretching vibration appears at 2900 cm^{-1}.
Sulfate and phosphate groups interact with each other when both are outside the first solvation shell of vanadium. The signal coming from this interaction is affected by the protonation of the two acids. The interaction between SO_4^{2-} and H_3PO_4 generates a peak at 2200 cm^{-1} (Scheme 1a of the manuscript). In contrast, in the case of HSO_4^- and H_3PO_4 we observe a signal at 3300 cm^{-1}. In the case of SO_4^- and $H_2PO_4^-$ the H-bond formed between the phosphate hydrogen and sulfate corresponds to a signal at 2900 cm^{-1}. Last, if HSO_4^- interacts with $H_2PO_4^-$ the signal produced by their interaction is at 3400 cm^{-1}. Raman wavenumbers at about 3600 cm^{-1} correspond to the O-H stretching of the HSO_4^- (Scheme 1b and 1d of the manuscript), while the ones at above 3700 cm^{-1} can be assigned to the internal O-H stretching of the H_2O molecules.

V^{3+}. As described in the manuscript, the configurations of V^{3+} show H-bonds between the H_2O molecules of the first solvation shell and the oxygens of the sulfate group (see Scheme 2 of the manuscript). As shown in Figure S9, The O-H stretching with the oxygen from the sulfate group produces a signal at 3000-3200 cm^{-1} in the Raman spectra. In this case however we did not notice any shift due to the presence of the H_3PO_4 in the first coordination shell. Passing to the bisulfate group, this signal covers a larger range of wavenumbers going from 3000 up to 3500 cm^{-1}. As for the V^{2+} case, in the range of 3400-3500 cm-1 a signal appears coming from the H-bonds formed between the H_2O molecules outside the first solvation shell and the sulfate or bisulfate group.
In contrast to V^{2+}, the signals coming from the H-bonding between H_2O molecules of the first shell and the H3PO4 are observed in two different possible ranges. If the bonding takes place between the water hydrogens and the oxygen from the deprotonated phosphoric acid, the signal appears in the range of 3000-3300 cm^{-1}. On the other hand, if the H-bonding involves an oxygen from the protonated H_3PO_4, the signal appears in the range of 3400-3600 cm^{-1}. When considering $H_2PO_4^-$, H-bonding occurs only between unprotonated oxygens and H_2O of the first solvation shell and the corresponding signals can span a very large range of wavenumbers, 2400-3300 cm^{-1}.
Finally, we noticed that the interaction between sulfate and phosphate groups also in this case varies depending on the sulfate-phosphate pair considered. The interaction between SO_4^{2-} and H_3PO_4 generates a peak at 2800 cm^{-1}. In the case of HSO_4^- and H_3PO_4 we observe a signal at 2600 cm^{-1}. In the case of SO_4^- and $H_2PO_4^-$ the H-bond formed between the phosphate hydrogen and sulfate corresponds to a signal of 3200 cm^{-1}. Last, if HSO_4^- interacts with $H_2PO_4^-$ the signal produced by their interaction appears at 3100 cm^{-1}.

VO^{2+}. All configuration of VO^{2+} (except for Confs 2 (Scheme 3.a of the manuscript), 4 (Scheme 3.c) and 2 (Scheme 3.d)) exhibit H-Bonds between the water molecules present in the first solvation shell of vanadium and the oxygen atoms of the sulfate/bisulfate group. As shown in Figure S10, the O-H stretching vibration arising from the sulfate group refers to a signal that span a broad range of wavenumbers, 2400-3100 cm^{-1}. However, as in the case of V^{2+}, we noticed that when $H_3PO_4/H_2PO_4^-$ is in the first coordination shell the signal appears to be shifted to 2200-2400 cm^{-1}. Again, as for the V^{2+} case, passing from the sulfate to the bisulfate group, this signal shifts to higher wavenumbers, 3300-3500 cm^{-1}. Moreover, also for the bisulfate, when $H_3PO_4/H_2PO_4^-$ is in the first coordination shell this signal moves to lower wavenumbers 3100-3200 cm^{-1}.
The signal due to the H-bonds formed between the H_2O molecules outside the first solvation shell and the sulfate or bisulfate group is different, in contrast with V^{2+} and V^{3+} cases. The first falls in the 3200-3500 cm^{-1} range, while the second in the 3500-3600 cm^{-1} range of the Raman spectra.
The signal coming from the H-bonding between H_2O molecules of the first shell and the H_3PO_4 or $H_2PO_4^-$, as in the V^{3+} case, fall in two possible ranges. On one hand, if the H-bonding involves a protonated H_3PO_4/ $H_2PO_4^-$ oxygen the signal falls in the 3400-3600 cm^{-1} range. On the other hand, if the bonding takes place between the water hydrogens and the unprotonated oxygen the signal falls in the 3000-3500 cm^{-1} wavenumbers range, in the case of H_3PO_4, and in the lower 2300-3200 cm^{-1} range in the case of $H_2PO_4^-$.
Sulfate and phosphate groups interact when both are outside the first solvation shell of vanadium. The signal coming from this interaction changes in correspondence of the protonation of the two acids. The interaction between SO_4^{2-} and H_3PO_4 generates a peak at 2400 cm^{-1}. In the case of HSO_4^- and H_3PO_4, we observe a signal at 3200 cm^{-1}. In the presence of SO_4^- and $H_2PO_4^-$, the H-bond formed between the phosphate hydrogen and sulfate corresponds to a signal of 3100 cm^{-1}. Last, if HSO_4^- interacts with $H_2PO_4^-$ the signal produced by their interaction is at 3500 cm^{-1}.

In contrast with the previous cases, we also observed some peaks corresponding to H-bonding between H_2O molecules or H_3PO4/H_2PO4^- and the oxygen of VO^{2+}. The corresponding signals were found at 3500 cm^{-1} in the case of H_2O, 3300-3500 cm^{-1} in the case of H_3PO_4 and 3650 cm^{-1} for $H_2PO_4^-$.

VO_2^+. The VO_2^+ case is the most particular one. In fact, several of the most stable structures changed the initial protonation arrangement during the geometry optimization (Scheme 4 of the manuscript). This gave rise to different combination of sulfate, bisulfate phosphoric acid and triphosphate pairs, as well as formation of H_3O^+ ions. Moreover, we found that several peaks correspond to combined H-bond stretching vibrations. In this framework, it was not possible to identify a common pattern in the spectra of the most stable V(V) configurations, as it was done in the previous cases.

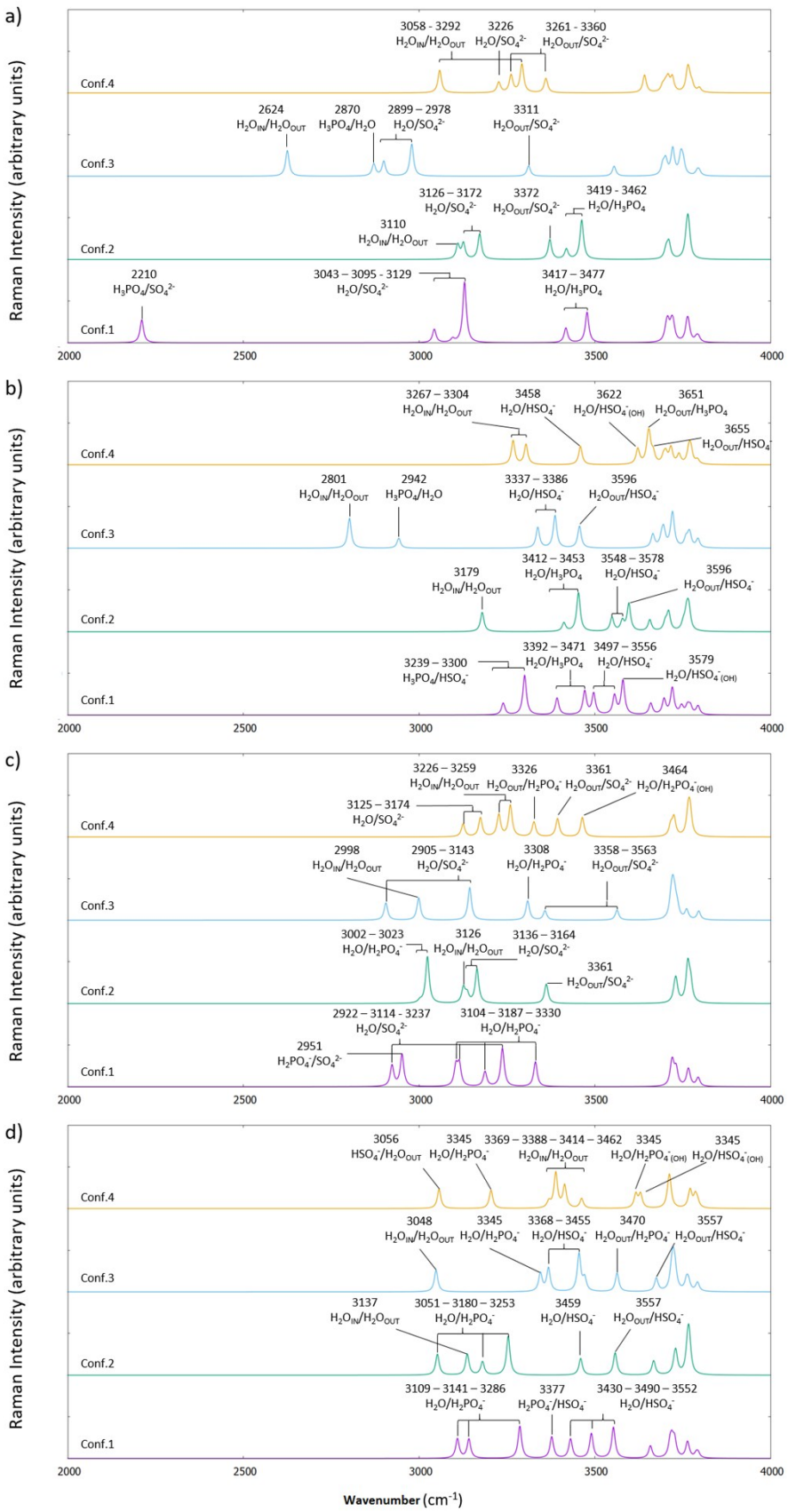

Figure S8. **a)** Computational Raman Spectra in the 2000-4000 cm^{-1} range for the V^{2+} cation within the vicinity of SO_4^{2-} and H_3PO_4. **b)** The protonation of SO_4^{2-} is considered. **c)** The deprotonation of H_3PO_4 is shown. **d)** The protonation of SO_4^{2-} and the first deprotonation of H_3PO_4 are here represented. The most significant structures are selected on the basis of Scheme S1.

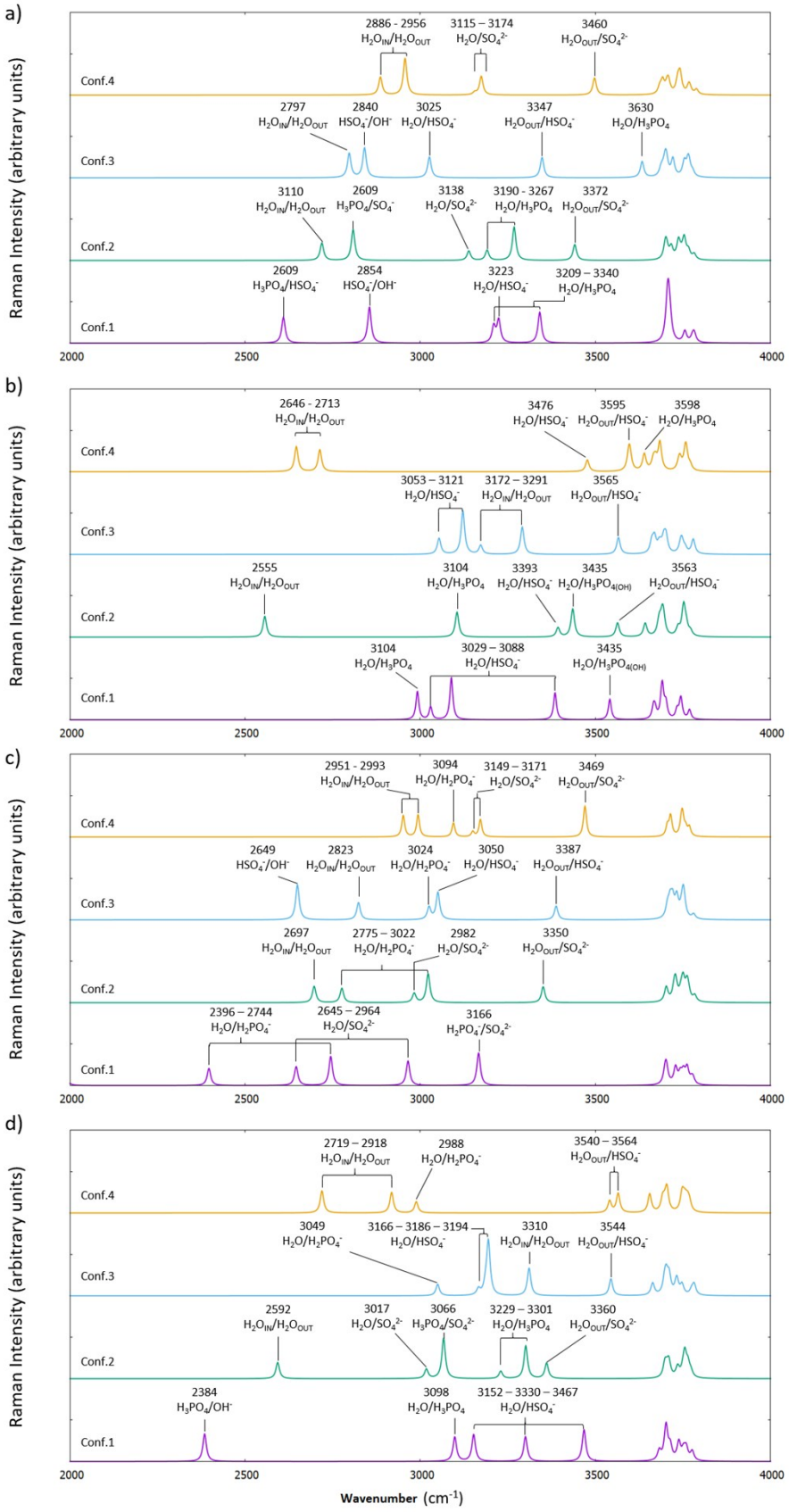

Figure S9. **a)** Computational Raman Spectra in the 2000-4000 cm^{-1} range for the V^{3+} cation within the vicinity of SO_4^{2-} and H_3PO_4. **b)** The protonation of SO_4^{2-} is considered. **c)** The deprotonation of H_3PO_4 is shown. **d)** The protonation of SO_4^{2-} and the first deprotonation of H_3PO_4 are here represented. The most significant structures are selected on the basis of Scheme S1.

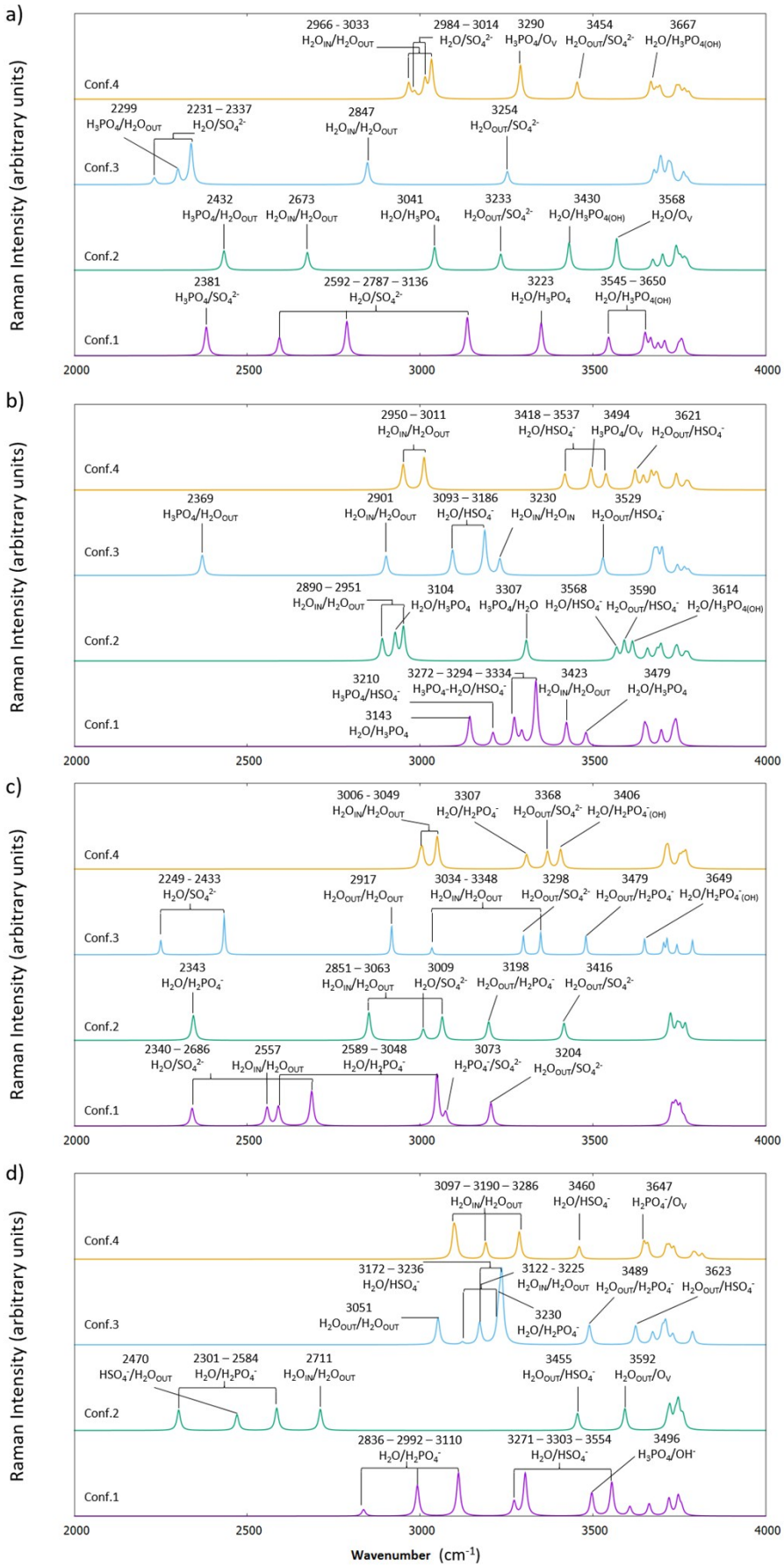

Figure S10. **a)** Computational Raman Spectra in the 2000-4000 cm^{-1} range for the VO^{2+} cation within the vicinity of SO_4^{2-} and H_3PO_4. **b)** The protonation of SO_4^{2-} is considered. **c)** The deprotonation of H_3PO_4 is shown. **d)** The protonation of SO_4^{2-} and the first deprotonation of H_3PO_4 are here represented. The most significant structures are selected on the basis of Scheme S1.

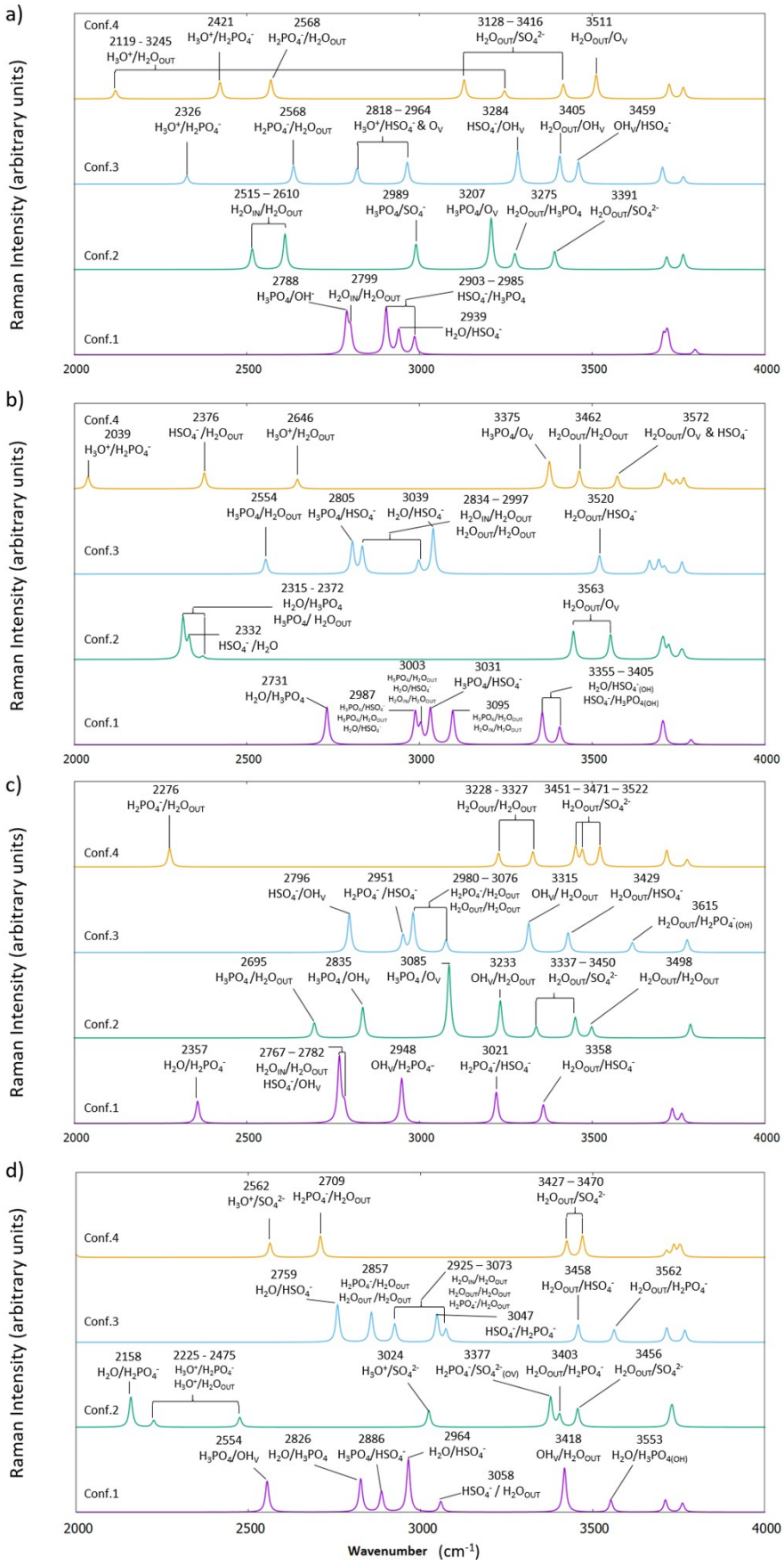

Figure S11. **a)** Computational Raman Spectra in the 2000-4000 cm^{-1} range for the VO_2^+ cation within the vicinity of SO_4^{2-} and H_3PO_4. **b)** The protonation of SO_4^{2-} is considered. **c)** The deprotonation of H_3PO_4 is shown. **d)** The protonation of SO_4^{2-} and the first deprotonation of H_3PO_4 are here represented. The most significant structures are selected on the basis of Scheme S1.

References

1 A. D. Becke, *J. Chem. Phys.,* 1993, **98**, 1372–1377.

2 Aleksandr V. Marenich, Christopher J. Cramer, Donald G. Truhlar, *J. Phys. Chem. B,* 2009, **113**, 6378–6396.

3 F. Sepehr, S. J. Paddison, *Chem. Phys. Lett.,* 2013, **585**, 53–58.

4 M. Frisch, G. Trucks, H. Schlegel, G. Scuseria, M. Robb, J. Cheeseman, J. Montgomery, T. Vreven, K. Kudin, J. Burant, et al., *Gaussian 03, Revision C.02*, n.d.

5 M. Bon, T. Laino, A. Curioni, M. Parrinello, *J. Phys. Chem. C,* 2016, **120**, 10791–10798.

6 M. Skyllas-Kazacos, L. Cao, M. Kazacos, N. Kausar, A. Mousa, *ChemSusChem,* 2016, **9**, 1521–1543.

7 G. Socrates, *Infrared and Raman Characteristic Group Frequencies: Tables and Charts*, John Wiley & Sons, 2001.

Author Contributions

Fabio J. Oldenburg and Marta Bon share the first authorship and carried out the experimental analysis and the DFT-calculations, respectively. Daniele Perego supported on the experimental side, in particular with measuring the electrochemical impedance spectroscopy on all half-cells and helped editing the manuscript. Daniela Polino supported on the theoretical side with calculating and interpreting the theoretical Raman-spectra that were used to verify the experimental analysis. Teodoro Laino, Thomas J. Schmidt and Lorenz Gubler guided and supported the work from the administrative side and supervised the work of Marta Bon and Fabio Oldenburg, respectively. They gave valuable advice for interpreting the data and writing the manuscript. They further acquired the required funding and defined the framework of this project.